Design and control of a novel bionic mantis shrimp robot

Gang Chen [a, c *], Yidong Xu [a], Chenguang Yang [b *], Xin Yang [a], Huosheng Hu [c], Xinxue Chai [a], Donghai Wang [a]

a Faculty of Mechanical Engineering and Automation, Zhejiang Sci-Tech University, Hangzhou 310018, China

b Bristol Robotics Laboratory, University of the West of England, Bristol BS16 1QY, U.K.

c School of Computer Science and Electronic Engineering, University of Essex, Colchester CO4 3SQ, U.K.

*Corresponding author, Email: gchen@zstu.edu.cn, Charlie.Yang@uwe.ac.uk

Abstract:

This paper presents the development of a novel bionic robot which is inspired by agile and fast mantis shrimps in the ocean. The developed bionic mantis shrimp robot has ten rigid-flexible swimming feet (pleopods) for swimming propulsion and a rope-driven spine for its body bending. A central pattern generator (CPG) is adopted to effectively imitate the swimming motion of a real mantis shrimp so that the robot can achieve a maximum swimming speed of 0.28m/s (0.46 body length per second) and a minimum turning radius of 0.36m. The influence of control parameters on the robot's swimming performance is then investigated. Experiments are conducted to show that the oscillation frequency of the bionic pleopod plays a major positive role in the robot's swimming speed. This study has demonstrated the effectiveness of the proposed mechanism design and motion control method for a bionic mantis shrimp robot and laid the foundation for the further exploration of bionic mantis shrimp robot in rugged seabed environments.

Keywords: bionic robot, mantis shrimp, gait planning, CPG control, rigid-flexible pleopod, rope-driven

1. Introduction

After a long time of environmental adaptation, the motion mechanism of organisms in nature is more advantageous than that of ordinary propeller propulsion. Marine organisms are capable of both fast swimming and agile maneuverability. As one of the most capable predators in shallow water, mantis shrimp is characterized by powerful forelimbs that produce bullet-like acceleration to deliver devastating blows to its prey targets in tropical and subtropical marine environments. Its swimming speed is extremely fast and can reach to a maximum speed of 30 body lengths per second. Its flat and bendable body structure can reduce fluid resistance and increase its maneuverability in swimming. The pleopod is the main source of thrust for a mantis shrimp. The flexible and multiple pair pleopods reduce drag and generate high propulsive forces. As shown in Fig. 1, a mantis shrimp attacked an octopus rapidly and suddenly, and eluded fast to avoid the attack from octopus, and finally the octopus chose to give up prey the

mantis shrimp and retreated.

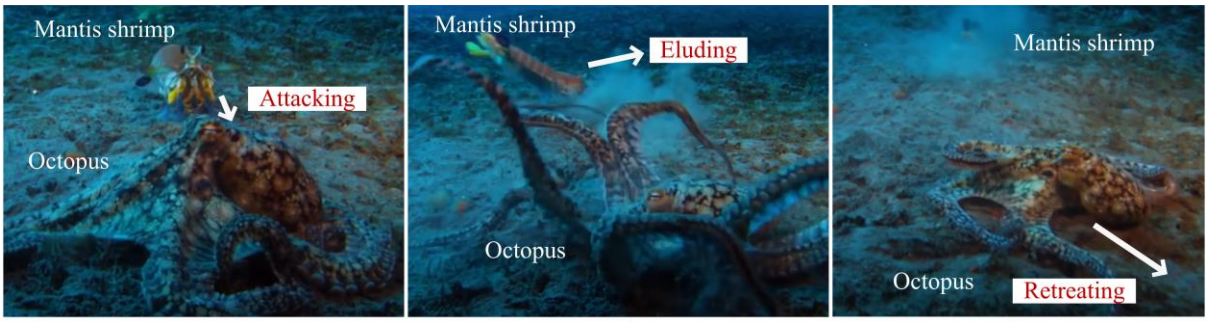

(a) (b) (c)

Fig. 1 A fight between a mantis shrimp and an octopus.

Based on marine organisms, some underwater bionic robots[1][2] have been developed for real-world applications, which have high mobility, adaptability, and excellent workability. For instance, the working principle of the predatory forelimb of mantis shrimp was investigated in [3] and computer vision was deployed for medical surgery based on its eye photosensitivity mechanism[4]. However, few research works were conducted on the motion structure and control so far.

Ford et al. studied the kinematics and hydrodynamics of shrimp [5] and completed kinematic planning and dynamic analysis based on hydrodynamic and particle flow. It was carried out on a fixed bench without a freely moving robot to verify its theory. Lim et al. proposed the use of a second harmonic-based trigonometric function to fit the motion of four pairs of pleopods of the American lobster [6]. However, this approach cannot be directly applied to the gait planning for a bionic mantis shrimp robot with different number of pleopods. Therefore, the study of the structure, motion planning and control of bionic mantis shrimp robot becomes necessary.

Central pattern generators (CPGs) are neural systems found in both invertebrate and vertebrate animals that can create rhythmic patterns of neural activity and then produce coordinated rhythmic movements [7-9]. As an invertebrate arthropod, a mantis shrimp swims mainly by the rhythmic movement of its pleopod and the flexion of its body. Many CPG-based motion control models have been established for bionic robots to realize various modes of motion control such as flying, jumping, walking, and running [10-13]. Rostro-Gonzalez et al. proposed a CPG controller for a hexapod robot[14], which cannot be directly used for the CPG motion control of a bionic mantis shrimp robot.

This paper aims to study the design and CPG motion control of a bionic mantis shrimp robot. We developed the agile robot with powerful propulsion by ten pleopods and flexible body and implemented its effective swimming motion by CPG controller. This study can provide new underwater platform for the detection of complex underwater environment. The rest of this paper is organized as follows. Section 2 presents the structure design of the proposed bionic mantis shrimp robot. In Section 3, the gait planning is proposed for the pleopod swimming of the bionic mantis shrimp robot based on the motion of a real mantis shrimp. Section 4 introduces the CPG control method used to control the proposed bionic mantis shrimp

robot. Experiments are conducted in Section 5 to verify the swimming performance of the bionic mantis shrimp robot. Finally, a brief conclusion and future work are given in Section 6.

2. Design of the bionic mantis shrimp robot

As shown in Fig.2 (a), a mantis shrimp consists of five main parts: head, carapace, walking feet, pleopods and telson. It uses its walking foot to crawl and relies on the paddling of pleopod to swim. Based on the physiological structure and movement characteristics of a mantis shrimp, we design a bionic mantis shrimp robot, which consists of four main parts: head, flexible body, bionic pleopod, and telson. The head of the robot, i.e., a waterproof box, has a built-in controller and is fixed to a carbon-fiber base. The flexible body consists of the wire rope, silicone spine and five propulsion segments.

A waterproof servo for pulling the wire rope is located in the carbon fiber base. A propulsion segment consists of a 3D printed segments base, two waterproof servos, and a three-joint bionic pleopod. The pleopod is 3D printed with elastic silicone film fixed by screws on one side and has two states (propulsion state and recovery state) when it moves forward and backward. The robot's telson is 3D printed and attached to the end of the elastic spine to hold the wire rope and is secured with a buoyancy material. The assembled prototype of the bionic mantis shrimp robot is shown in Fig.2 (b).

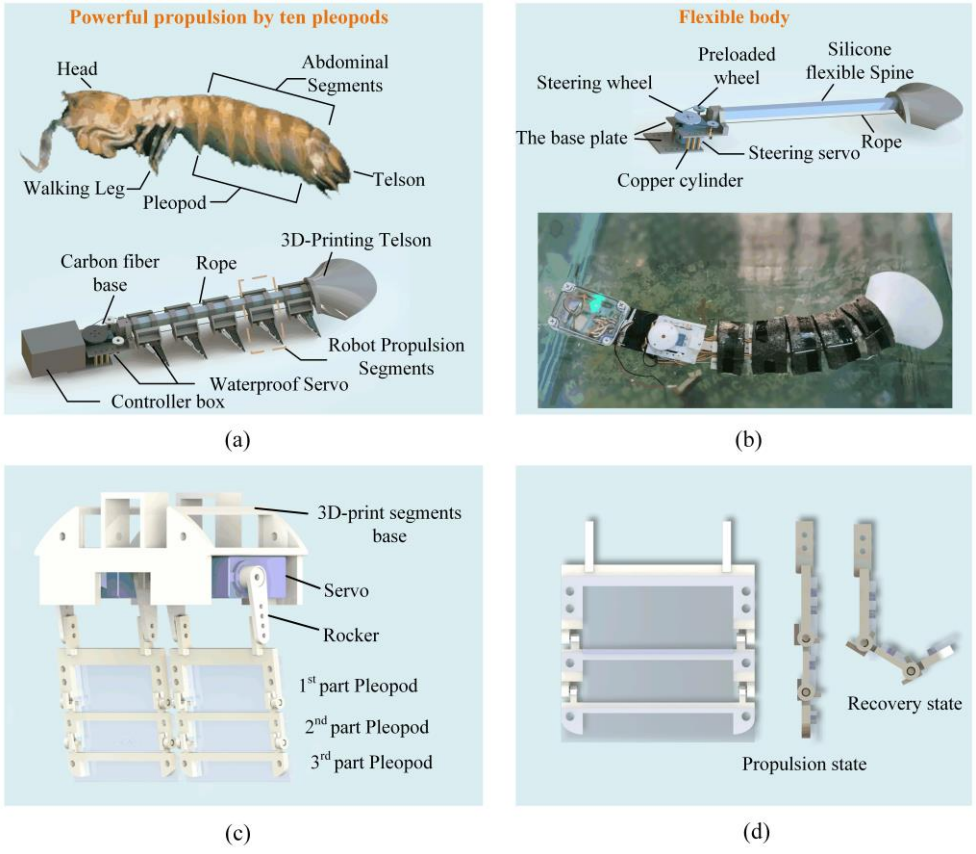

Fig. 2 Mantis shrimp and bionic mantis shrimp robot. (a) Mantis shrimp and robot model. (b) Bionic mantis

shrimp robot platform. (c) Robot's propulsion segment. (d) Pleopod and its two working states.

Fig.2 (c) shows the structure of a single propulsion segment of a bionic mantis shrimp robot with a pair of waterproof servos and two pleopod mechanism. The waterproof servo drives the pleopod mechanism in the working plane by means of a 3D-printed rocker arm to perform reciprocating rotation movements. Fig.2 (d) shows the two states of the robot's pleopod: propulsion state and recovery state. In nature, the pleopod of a mantis shrimp also has these two main states when swimming, which provides greater forward propulsion while reducing the forward resistance to pleopod in recovery. The bionic pleopod consists of a 3D-printed frame with an elastic silicone film and the passive joints on the frame are limited so that it can paddle as a biological pleopod without an active actuation.

The bending of the robot is achieved by a steering servo and a rope traction device[15]. The wire rope starts from the steering servo and passes through propulsion segments one by one and is finally fixed at the telson. When the steering servo rotates, it can drive the silicone spine to bend. Table 1 shows the design parameters of the developed robot.

Table 1 Design parameters of the robot

Design Parameter	Value (mm）
Prototype robot (length*width*height)	600*65*75
Segments base (length*width*height)	42*78*34
Distance between segments base	14
Robot pleopod (length*width*height)	45*42*2
Silicone spine (length*width*height)	350*15*15
Controller box (length*width*height)	95*55*65

3. Swimming gait planning of the robot

For a bionic mantis shrimp robot, the swimming gait planning of its bionic pleopod plays a key role to achieve its bionic swimming capabilities. Based on a video clip of a mantis shrimp swimming in water, the pleopod motion was analyzed and modeled to obtain its kinematic equations. The paddling angle of the pleopod is defined as shown in Fig.3 (b). Its raw sampling data is shown in Fig.3 (a), where the x and y represent time and paddling angle of the pleopod.

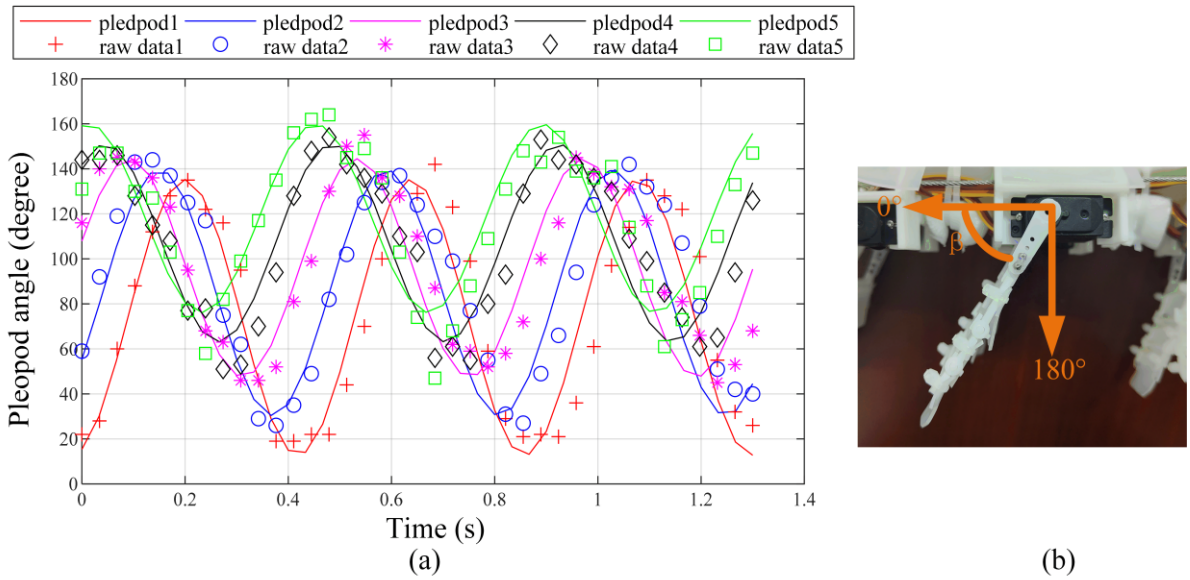

Fig. 3 Swimming trajectories of mantis shrimp. (a) Sampling results from swimming video of mantis shrimp and its fitting trajectory curve. (b) Paddling angle definition of the pledpod.

Using the cftool toolbox[16] in Matlab to fit the sampled points, the swimming trajectories of pleopods can be obtained, where the R-square between each fitted curve and its original data point is above 0.9. The fitting function is as follows.

$$\beta_i(t) = a_i + b_i \cdot cos(\omega t) + b_i sin(\omega t), 1 \le i \le 5 \quad (1)$$

where $\beta(t)$ is the swimming angle, ω is the frequency factor, i is the index of pleopod, a_i, b_i, and c_i are the magnitude coefficients of the constant, sine and cosine terms of the fitting function. The gait planning parameters for each bionic pleopod swimming gait are shown in Table 2.

Table 2 Parameters of the swimming trajectories of pleopods

Index of Pleopod	Parameters		
i	a	b	c
1	74	-61	-6
2	85	45	31
3	96	-7	48
4	107	22	38
5	118	35	23

As shown in Fig.3 (a), the fitting trajectories of the five pairs of pleopod represented by the curves pleopod 1-5 can be used as a basis swimming gait planning result for the bionic mantis shrimp robot.

4. CPG-based locomotion control

Based on the swimming trajectories of pleopods and the results in [17], we proposed a CPG controller for the rhythmic swimming of our bionic mantis shrimp robot. The CPG oscillator model for our bionic mantis shrimp robot can be described as follows.

$$\dot{\theta}_i = \omega_i + \sum_j r_{1j} w_{ij} \sin\left(\theta_j - \theta_i - \varphi_{ij}\right) \tag{2}$$

$$\ddot{r}_{1i} = \alpha_i\left(\frac{\alpha_i}{4}\left(R_{1i} - r_{1i}\right) - \dot{r}_{1i}\right) \tag{3}$$

$$\ddot{r}_{2i} = \alpha_i\left(\frac{\alpha_i}{4}\left(R_{2i} - r_{2i}\right) - \dot{r}_{2i}\right) \tag{4}$$

$$\ddot{x}_i = \alpha_i\left(\frac{\alpha_i}{4}\left(X_i - x_i\right) - \dot{x}_i\right) \tag{5}$$

$$\beta_i = x_i + r_{1i}\cos(\theta) + r_{2i}\sin(\theta) \tag{6}$$

where ω_i is the desired frequency of the oscillator. x_i, r_{2i}, and r_{1i} are the amplitude state variables of the output deviation term, sine term and cosine term in the oscillator *i*. α_i is constant positive gains. w_{ij} and φ_{ij} are parameters respectively coupling weights and phase biases which determine how oscillator j influences oscillator *i*. R_{1i}, R_{2i}, and X_i are parameters of controller representing the desired amplitude of each corresponding output term of the oscillator. β_i represents the final output angle of each oscillator.

The oscillator output model can easily fit the motion characteristics of the bionic mantis shrimp robot according to the gait planning parameters. In addition, the model inherits the characteristics of the Ijspeert oscillator[12], which can directly adjust the frequency and phase difference of several amplitude parameters. Fig. 4 shows the effect results of oscillator parameters on output of a single CPG oscillator. In Fig. 4, the number of cycles of the CPG operation is used as the horizontal axis and the output angle of the oscillator is used as the vertical axis, the dotted line represents the node where the parameter changes and the blue curve is the actual output of the oscillator.

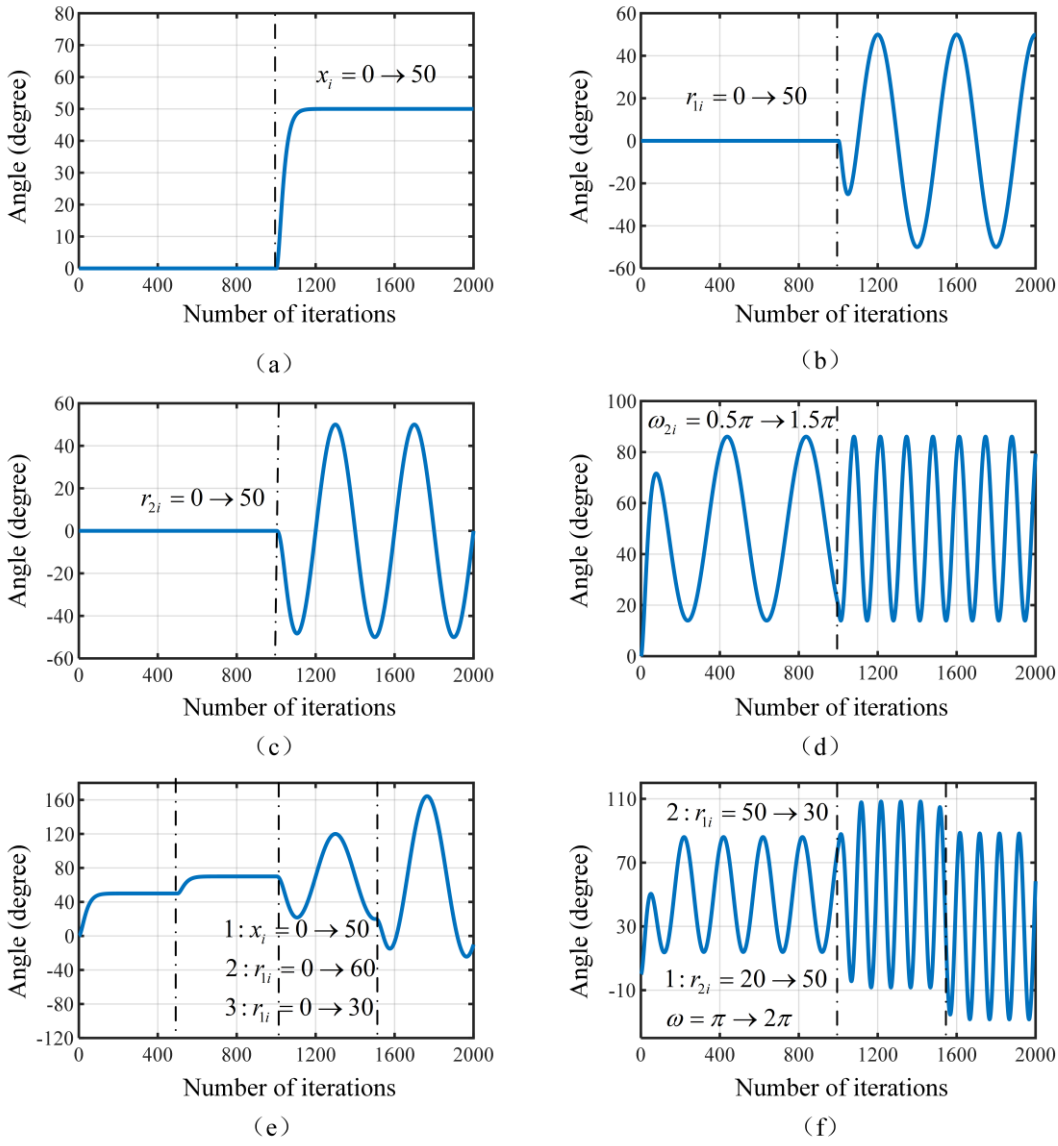

Fig. 4 Effect of CPG parameters on single CPG output. (a) Effect of x_i on CPG output. (b) Effect of r_{1i} on CPG output. (c) Effect of r_{2i} on CPG output. (d) Effect of ω on CPG output. (e) Effect of x_i, r_{1i}, r_{2i} on CPG output. (f) Effect of x_i, r_{2i}, ω on CPG output.

Fig. 4 (a), (b), and (c) show the output of the oscillator when only the constant, sine or cosine term coefficients of the adjusted output are changed individually. Fig. 4(d) shows that the output frequency of the oscillator can be changed correspondingly by modifying the expected frequency of the oscillator. Fig. 4(e) and (f) show that appropriate changes to multiple parameters of the oscillator can achieve dynamic adjustment of the output without affecting the effectiveness of the oscillator output.

These results show that the output of a CPG oscillator can be configured to match the gait planning of robot, thus implementing the motion of the bionic pleopod. The frequency of the CPG oscillator can also be varied by adjusting the desired frequency parameter, which can be used to adjust the motion frequency of the bionic pleopod.

A single CPG oscillator is typically used to generate rhythmic control signals for a single joint. The bionic mantis shrimp robot has 10 independently controllable bionic pleopods and a rope-driven-based flexible spine. Based on these characteristics, a CPG network model for the bionic mantis shrimp robot should be constructed, which can output multiple control signals through the configuration of coupling parameters for agile swimming of the robot.

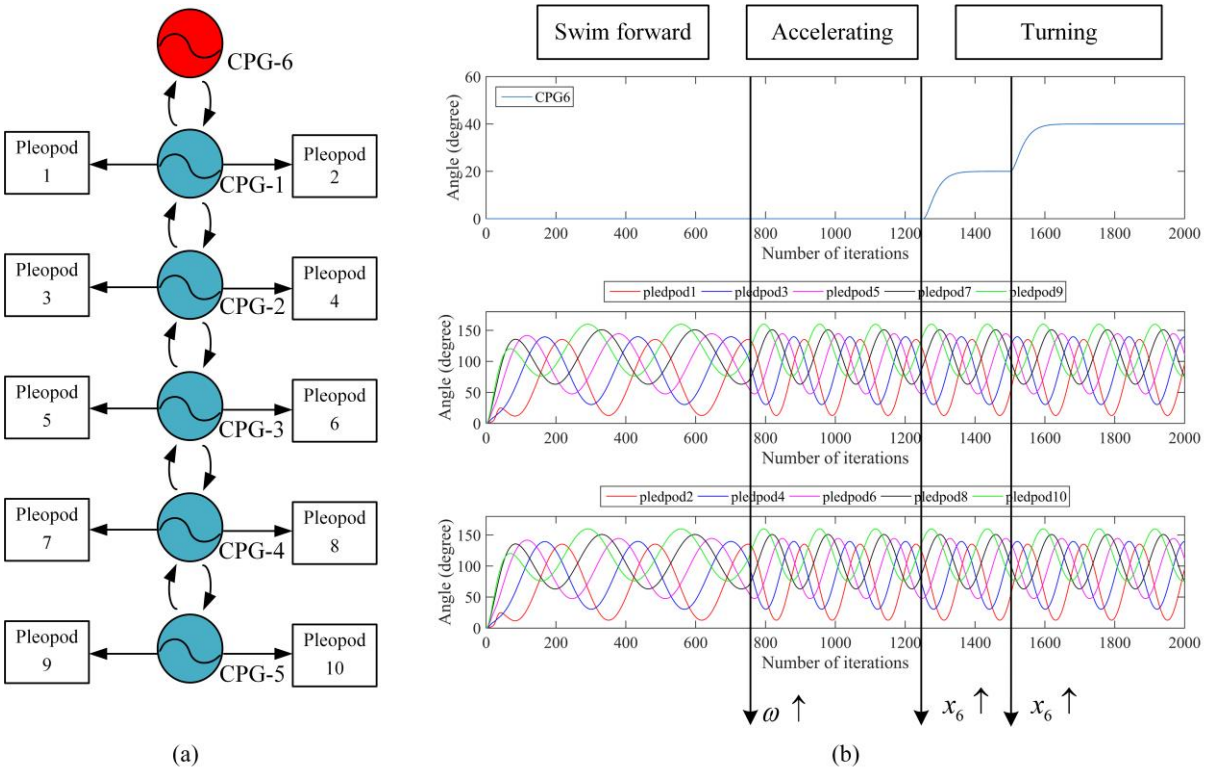

Fig. 5 CPG network and its outputs.(a) CPG network used for robot control. (b) Outputs of CPG 6 and pleopod 1-10 in different locomotion status.

Fig.5 (a) illustrates the topology of the CPG network consisting of 6 mutually coupled oscillators. CPG-1 to CPG-5 are used to configure the reference output angles of the five pairs of bionic pleopod, whose parameters are determined according to the values in Table 2. CPG-6 is used to configure the output angle of the steering servo and can be used for the bionic mantis shrimp robot after a reasonable configuration of parameters and can achieve the straight swimming and turning motion mode. Fig.5 (b) shows the output of the CPG-6 controller.

In the straight motion, the output of CPG-6 is always zero and the left and right pleopods are output at the same angle based on the same CPG, producing a balanced and forward propulsion force. In the turning motion, the output of CPG-6 is not zero and drives the central servo to pull the flexible spine to bend. At this time, each bionic pleopod maintains its original paddling state to generate torque for turning motion.

In the CPG network, phase differences in the pleopod motion are achieved by parameter configuration of the output item. Test results show that the desired bionic pleopod gait is obtained when φ is 0. In addition, it was found that there is a relationship between the value

of the weight coupling parameter φ and the desired frequency of oscillator ω. Its ratio is defined as the lagging parameter L:

$$L = \frac{\varphi}{\omega} \tag{7}$$

Varying the value of the coupling weights φ_{ij} according to the desired frequency ω creates an additional phase difference between adjacent oscillators. Fig. 6 shows the effect of weighted coupling parameter on output of the CPG oscillator. The outputs of CPG-1 to CPG-5 are shown in Fig. 6(a) and (b) when the ratio L is 0 and 0.2. The output of CPG-1 oscillator is plotted in Fig. 6(c) with L values: 0, 0.1, 0.2 and 0.4. When L is from 0 to 0.2, the output of the CPG network model can maintain the basic form of the gait planning, and the phase difference between adjacent CPG oscillators increases with the value L. When the value L continues to increase to over 0.2, CPG-4 coincides with the output of next oscillation cycle. At this time, the output of the CPG network model is no longer consistent with the gait planning result, and the wrong motion state of pleopod may be generated, resulting in the collision of front and rear bionic pleopods.

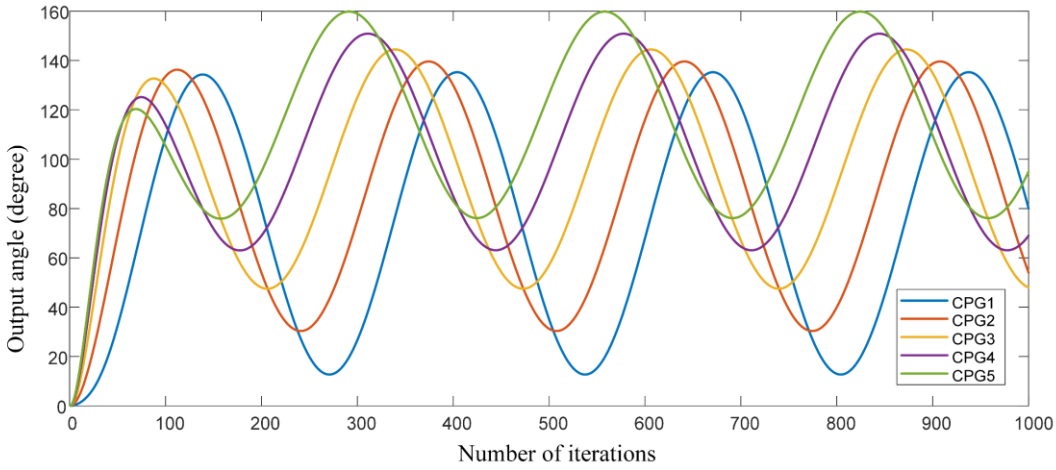

(a)

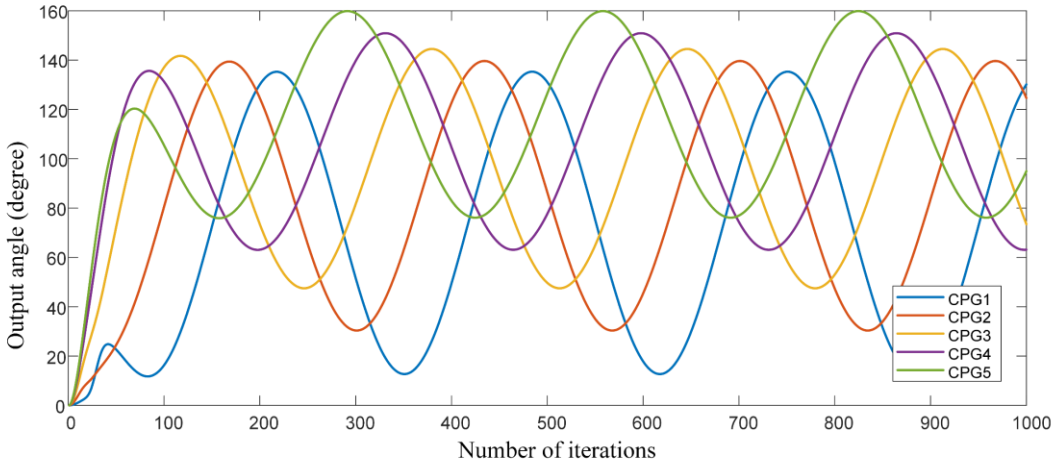

(b)

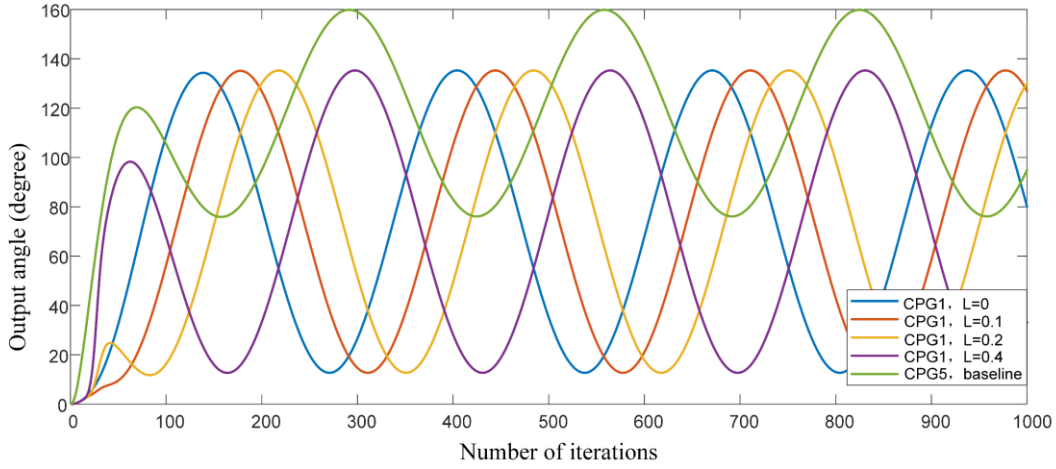

（c）

Fig. 6 Effect of L to the output of CPG network. (a) The CPG 1~5 output when L=0 (b) The CPG 1~5 output when L=0.2 (c) The CPG 1 output when L=0,0.1,0.2,0.4, CPG 5 is the baseline.

5 Experiments

An experimental platform was built for robot swimming experiments in order to verify the effectiveness of the proposed robot structure, gait planning and CPG controller. Fig.7 shows

the water tank and sensors used for the experiment. The size of water tank is 2.0m length, 1.0m width, and 1.0m height. A camera is used to record robot's movement and a laser ranging sensor is used to detect the robot's movement in the straight swimming experiment.

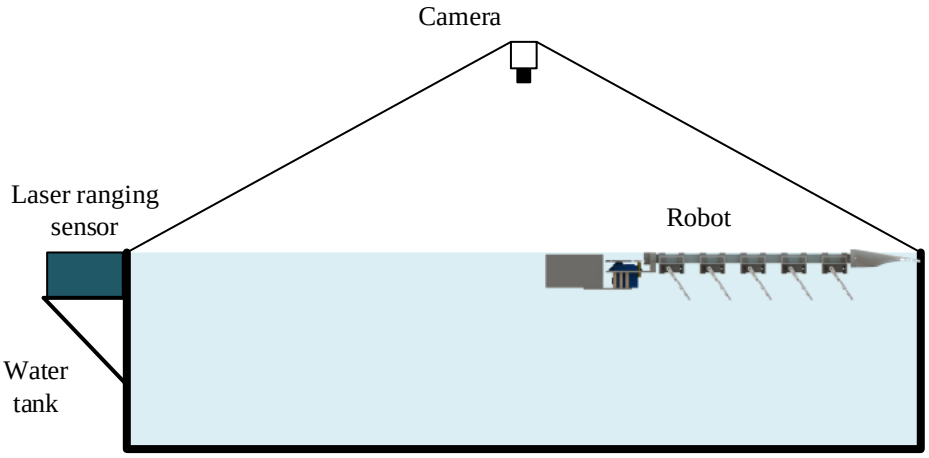

Fig. 7 Experimental platform and equipment

A. Forward straight swimming with different CPG parameters

As the swimming speed is a core indicator, this experiment aims to investigate the effect of the robot's CPG parameters on its swimming speed. In the experiment, the steering servo of our bionic mantis-like shrimp robot does not rotate, remaining in its initial position, and the robot relies on the thrust generated by the bionic pleopod to achieve forward swimming. The laser ranging sensor was used to measure the robot's motion position and calculate the average speed of the robot in one swimming cycle from one end of the water tank to the other end.

Fig. 8 shows the experimental results, in which Z-axis represents the measured average speed of the robot, X-axis represents the desired frequency of the oscillator and Y-axis is the lagging parameter L, twenty-eight sets of experiments were completed, each of which was repeated three times to avoid the effect of chance. The average value was taken as the result of each set of experiments.

The previous sections showed that changing the lagging parameter produces an additional phase difference between neighboring CPG oscillators. Here, the experimental results show that when the oscillation frequency is increased, the average speed of the robot's movement is also increased. However, the effect of the lagging parameter on the speed is not obvious, but the overall trend can be observed as the speed tends to decrease and then increase when increasing from 0.

In the experiment, the maximum average speed of the robot in the water tank was measured to be approximately 0.12m/s and the maximum speed that could be achieved after sufficient acceleration was approximately 0.28m/s (0.46 body length per second).

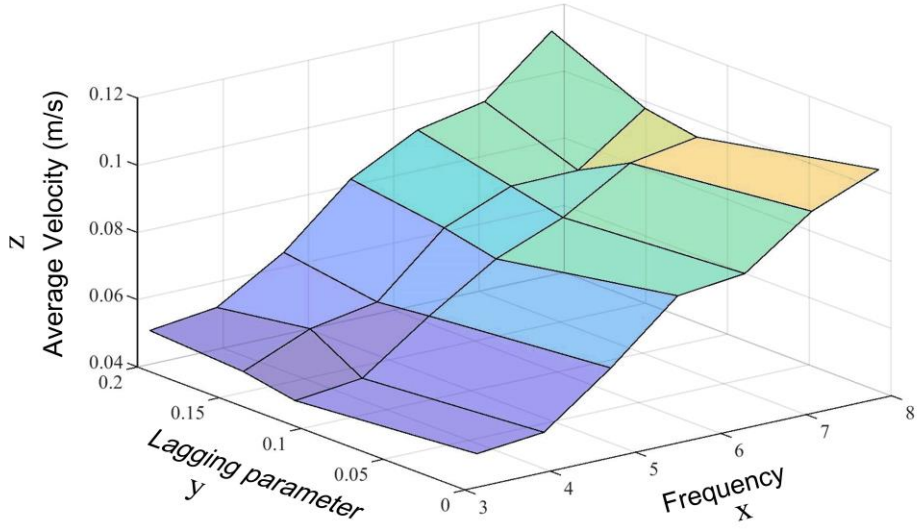

Fig. 8 Effect of CPG parameter on swimming speed

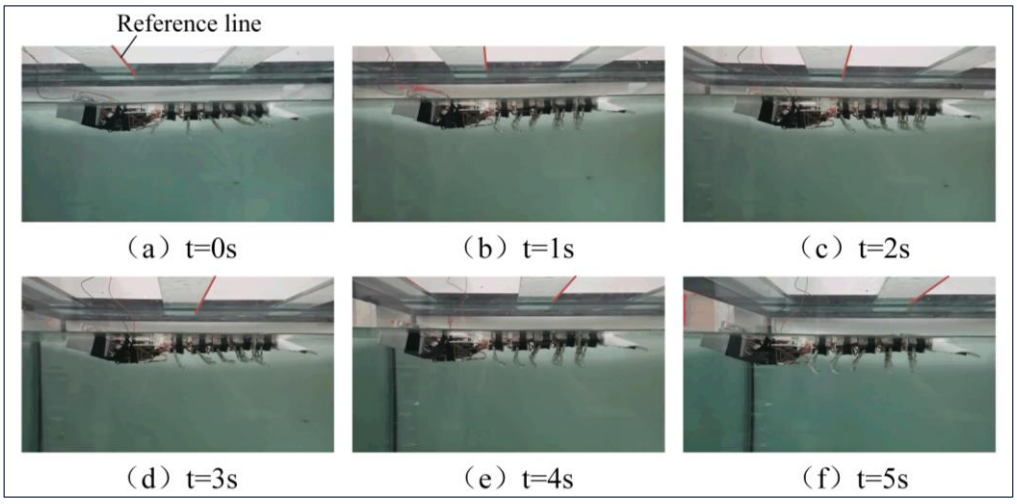

Fig. 9 Moving image sequence

B. Swimming experiments with variable lagging parameters

In this experiment, the experimental environment is set up in the same way as in experiment A. The robot will complete its motion at the same desired frequency, based on different phase parameters, and the frequency is both set to 2.5π. The lagging parameter for experiment 1 is 0 while the lagging parameter for experiment 2 is 0.2. Fig.10 shows the experimental results. The experimental results for relative distance, velocity, and acceleration for experiment 1 and experiment 2 are given in Fig.10 (a), (b) and (c) respectively.

As the experimental result show, the robot achieves a maximum instantaneous speed 0.28 m/s and an average speed 0.1 m/s with the lagging parameter set to 0. The acceleration data in Fig.10 (c) show that the robot has two sudden accelerations in the middle of the motion. It can be speculated that when the phase parameter is 0, the phase difference between the front and rear pleopods is small and the motion is more intensive, which can generate more propulsion

and impact the motion stationarity. When the lagging parameter is 0.2, the phase difference between the front and rear pleopods is large. Thus, the robot's velocity exhibits a periodic variation and is smoother, i.e., speed2 in Fig.10 (b).

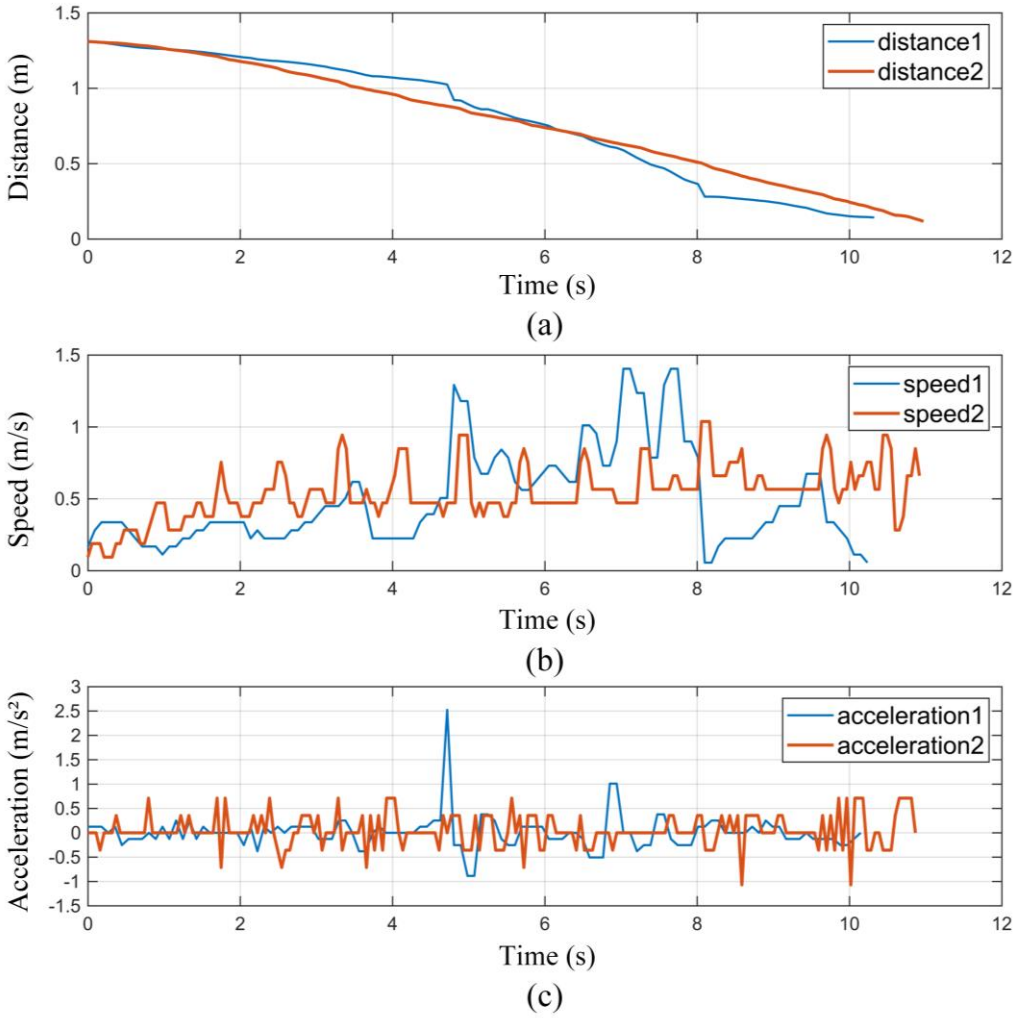

Fig. 10 Position, velocity, and acceleration of robot when the lagging parameters L is 0 (blue) and 0.2 (red).

C. Forward swimming and turning locomotion

In this experiment, the robot relies on the bionic pleopod to generate thrust and is adjusted by steering servo for turning movements. The CPG-6 parameters in the CPG network is adjusted and the robot completes a continuous series of swim motions in the water tank with a camera to record the robot's movements.

Fig.11 (a) shows the turning motion of our bionic mantis shrimp robot in the water tank. It took 7.8s to travel 1.02m distance, and therefore its average speed was 0.14m/s. Its turning radius was about 0.45m. Fig.11 (b) shows the two turning motions of the robot. The whole movement process took 23s, the total distance was 1.52m, and the average speed was 0.06m/s. The first turning radius was 0.36m, and the second turn radius was 0.41m.

As the experimental results show, our bionic mantis shrimp robot has good turning

capability in water and sufficient potential to be used for complex underwater navigation tasks. During the experiments, the robot was found to roll sideways, which was caused by excessive body lateralization when the robot conducted high maneuver turning, proposing a challenge for future research on attitude control of bionic mantis shrimp robots.

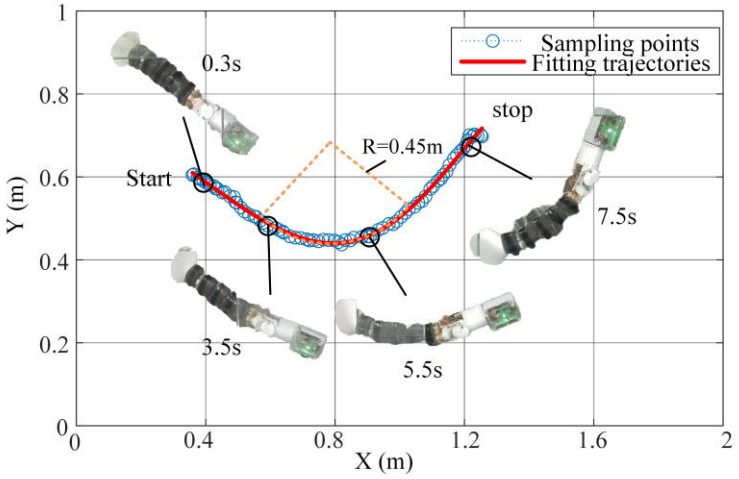

(a)

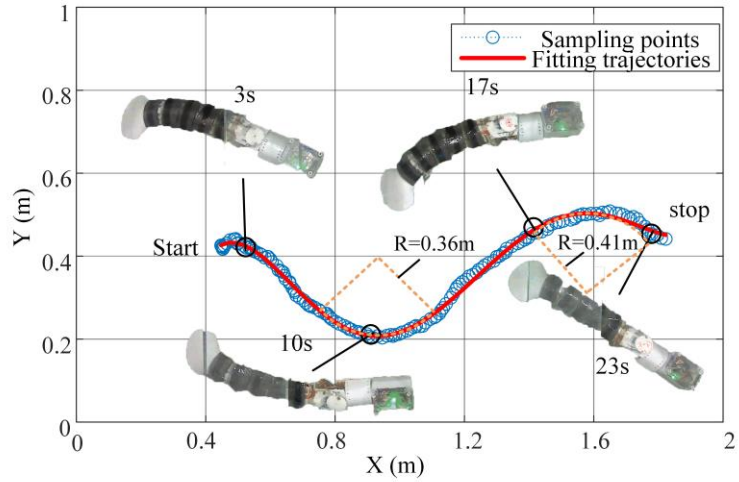

(b)

Fig. 11 Turning motion experiments of the robot. (a) One truning experiment. (b) Continuous turning experiment.

Based on the experimental results above, the following conclusions can be drawn:

(1) By increasing the motion frequency of the bionic pleopod, the average speed of the robot was increased from 0 to 0.12 m/s with the maximum frequency 3π in the experiment.

(2) Varying the lagging parameter in CPG, i.e., changing the phase difference between the pleopod pairs of motions, had little effect on the average robot speed theoretically. But in practical, the lagging parameters could affect the instantaneous speed and posture of the robot. When the lagging parameter was small, the robot exhibited faster instantaneous velocities and more unstable posture with a maximum instantaneous velocity of 0.28 m/s (0.46 BLS/s). However, the opposite results were observed when the phase difference was increased. This

result demonstrated that the bionic mantis shrimp robot can operate in both burst and smooth swimming states, presenting the potential bionic locomotor capabilities of the robot.

6 Conclusion and Future Work

Inspired by nature, a bionic mantis shrimp robot with bionic pleopods and rope-driven spine was developed in this paper. The swimming gait planning method and a CPG-based motion control system were investigated, including the effect of different control parameters on the robot's swimming speed. Experiments verified that the design of the bionic pleopod can provide sufficient propulsion for the robot to move forward and the rope-driven elastic spine can effectively realize the flexible turning of the robot. The results are given to show that the CPG-based robot motion control system can control the bionic mantis shrimp robot to move straight and turn. With two model parameters, the robot can be adjusted for straight and turning movements as well as acceleration and deceleration. It was found that too fast motion frequency of bionic pleopods may cause structural damage of the robot.

As pleopods can generate both forward propulsion and upward propulsion [18], our future research will be focused on investigating how to efficiently use of the propulsion generated by pleopods and how the robot can swim in narrow spaces safely.

Acknowledgements

This work was financially supported by National Natural Science Foundation of China (Nos. 51875528 and 41506116), Zhejiang Provincial Natural Science Foundation of China (Nos. LY20E050018 and LTY21F030001), the Key Research and Development Project of Zhejiang Province (No. 2021C04017), and Science Foundation of Zhejiang Sci-Tech University (ZSTU) (No. 17022183-Y).

References

[1]. Zhou, P.J., et al., Overview of Progress in Development of the Bionic Underwater Propulsion System. Journal of biomimetics, biomaterials and biomedical engineering, 2017. 32: p. 9.

[2]. Yu, J., et al., Motion Control and Motion Coordination of Bionic Robotic Fish: A Review. Journal of Bionic Engineering, 2018. 15(4): p. 579-598.

[3]. DeVries, M.S., E.A.K. Murphy and S.N. Patek, Strike mechanics of an ambush predator: the spearing mantis shrimp. Journal of Experimental Biology, 2012. 215(24): p. 4374-4384.

[4]. Blair, S., et al., Hexachromatic bioinspired camera for image-guided cancer surgery. Science Translational Medicine, 2021. 13(592): p. eaaw7067.

[5]. Ford, M.P., et al., Hydrodynamics of metachronal paddling: effects of varying Reynolds number and phase lag. royal society open science, 2019. 6(10): p. 191387-191387.

[6]. Lim, J.L. and M.E. DeMont, Kinematics, hydrodynamics and force production of pleopods suggest jet-assisted walking in the American lobster (Homarus americanus). Journal of Experimental Biology, 2009.

212(17): p. 2731-2745.
[7]. Ijspeert, A.J., Central pattern generators for locomotion control in animals and robots: a review. Neural networks, 2008. 21(4): p. 642-653.
[8]. Grillner, S., Neurobiological bases of rhythmic motor acts in vertebrates. Science, 1985. 228(4696): p. 143-149.
[9]. Orlovsky, T.G., et al., Neuronal control of locomotion: from mollusc to man. 1999: Oxford University Press.
[10]. Saputra, A.A., et al., AQuRo: A Cat-like Adaptive Quadruped Robot With Novel Bio-Inspired Capabilities. Frontiers in Robotics and AI, 2021. 8: p. 35.
[11]. Xie, F., et al., Central pattern generator (CPG) control of a biomimetic robot fish for multimodal swimming. Journal of Bionic Engineering, 2019. 16(2): p. 222-234.
[12]. Ijspeert, A.J., et al., From swimming to walking with a salamander robot driven by a spinal cord model. science, 2007. 315(5817): p. 1416-1420.
[13]. Spröwitz, A., et al., Towards dynamic trot gait locomotion: Design, control, and experiments with Cheetah-cub, a compliant quadruped robot. The International Journal of Robotics Research, 2013. 32(8): p. 932-950.
[14]. Rostro-Gonzalez, H., et al., A CPG system based on spiking neurons for hexapod robot locomotion. Neurocomputing, 2015. 170: p. 47-54.
[15]. Zhong, Y., Z. Li and R. Du, A Novel Robot Fish With Wire-Driven Active Body and Compliant Tail. ieee asme transactions on mechatronics, 2017. 22(4): p. 1633-1643.
[16]. Zhang Y, Ding C, Wang J, et al. High-energy orbit sliding mode control for nonlinear energy harvesting[J]. Nonlinear Dynamics, 2021, 105(1): 191-211.
[17]. Crespi, A., et al., Controlling swimming and crawling in a fish robot using a central pattern generator. autonomous robots, 2008. 25(1): p. 3-13.
[18]. Ford, M.P. and A. Santhanakrishnan, On the role of phase lag in multi-appendage metachronal swimming of euphausiids. Bioinspiration & Biomimetics, 2021. 16(6): p. 066007.